Inorganics **2014**, *2*, 211-232; doi:10.3390/inorganics2020211

OPEN ACCESS

inorganics

ISSN 2304-6740

www.mdpi.com/journal/inorganics

Article

IF-WS_2/Nanostructured Carbon Hybrids Generation and Their Characterization

Claudia C. Luhrs *, Michael Moberg, Ashley Maxson, Luke Brewer and Sarath Menon

Mechanical and Aerospace Engineering Department. Naval Postgraduate School 700 Dyer Rd. Watkins Hall. Monterey, CA 9394. USA; E-Mails: michael.moberg.2011@gmail.com (M.M.); ashley.r.maxson@gmail.com (A.M.); lnbrewer@nps.edu (L.B.); skmeno1@nps.edu (S.M.)

* Author to whom correspondence should be addressed; E-Mail: ccluhrs@nps.edu; Tel.: +1-831-656-2568.

Received: 5 March 2014; in revised form: 24 April 2014 / Accepted: 28 April 2014 / Published: 9 May 2014

Abstract: With the aim to develop a new generation of materials that combine either the known energy absorbing properties of carbon nanofibers (CNF), or the carbon-carbon bond strength of graphene sheets (G), with the shock resistance properties reported for Inorganic Fullerene type WS_2 structures (IF-WS_2), hybrid CNF/IF-WS_2 and G/IF-WS_2 were generated, characterized and tested. Experimentation revealed that *in situ* growth of carbon nanostructures with inorganic fullerene tungsten disulfide particulates had to be performed from particular precursors and fabrication conditions to avoid undesirable byproducts that hinder fiber growth or deter graphene generation. The novel protocols that allowed us to integrate the IF-WS_2 with the carbon nanostructures, producing dispersions at the nanoscale, are reported. Resulting hybrid CNF/IF-WS_2 and G/IF-WS_2 products were analyzed by X-ray Diffraction (XRD), Scanning Electron Microscope (SEM) and TEM (Transmission Electron Microscopy). The thermal stability of samples in air was evaluated by Thermogravimetric Analysis (TGA). CNF/IF-WS_2 and G/IF-WS_2 hybrids were introduced into epoxy matrices, and the mechanical properties of the resulting composites were analyzed using nanoindentation. Epoxy composite samples showed drastic improvements in the Young's modulus and hardness values by the use of only 1% hybrid weight loadings. The carbon nanofiber inclusions seem to have a much greater impact on the mechanical properties of the composite than the graphene based counterparts.

Keywords: IF-WS_2; carbon nanostructures; WS_2 composites; CNF/IF-WS_2; graphene/IF-WS_2

1. Introduction

Tungsten disulfide inorganic fullerene-like particulates (IF-WS_2), a dichalcogenide with distinct physical and chemical properties [1,2] that presents a hollow cage structure with potential uses as lubricant, component in batteries, supercapacitors or catalyst, among others [3–9], was introduced a few years ago as a material with shock resistance properties [10–13]. The shock absorbing ability of IF-WS_2 particulates allows them to endure pressures up to 25 GPa, with concomitant temperatures of up to 1000 °C, without structural degradation or phase change [12], a characteristic that opens an exciting window of possibilities for protective systems applications. Recent reports have further explored the features of such WS_2 nanostructures and some studies of their inclusion in polymeric matrices, along with the composites mechanical properties, have been published [14–24]. Despite those outstanding characteristics, the WS_2 density might be considered a drawback if it is to be used as component in protective gear that should be lightweight, able to withstand high temperatures and be flame resistant. A possible compromise between all those requirements might be made by joining the sought-after shock absorbing attribute of IF-WS_2 with lighter materials.

Due to their strength and light weight, tridimensional carbon assemblies and porous carbon structures such as nanotubes, foams or intertwined nanofibers [25–37], along with two-dimensional structures, such as Graphene [38–40], have been the focus of attention for energy absorbing applications. However, despite the advances in the field, the performance of personal protective equipment or sporting gear composed of carbon nanostructures can still be improved by the use of materials that could divert, distribute or dissipate the energy of impacts and the shock waves associated with them, in a more efficient manner.

Given the shock resistance characteristics of IF-WS_2 and the energy absorption of carbon nanostructures mentioned above, the combination of those two types of materials seems as a natural next step in the design of protective systems. Recent work that has successfully explored the possibility of merging the carbon component with IF-WS_2 using polymeric matrices [16,18,41–45]. However, the energy dissipation characteristics of those products could be attributed, to an extent, to the role of the viscoelastic polymeric matrices. Conversely, new reports in the generation of carbon fiber tridimensional structures have proven that CNF can be grown to form a macroscopic foam with viscoelastic properties without the need of a polymeric component [46]. Adding the known shock absorbing characteristics of IF-WS_2 to such type of carbon structures will be highly desirable and is the focus of this investigation.

The development of a protocol to combine the IF-WS_2 characteristics with those of the carbon structures in the absence of a polymer, to generate a random distribution of those two phases at the nanoscale (*ca.* a hybrid made of solely inorganic components, thus, avoiding some of the polymer drawbacks such as aging but gaining in terms of lightweight and thermal stability), remains as one of the major challenges.

Experimentation by our group has shown that adding IF-WS_2 to an already existing 3D carbon structure, even when using solvents to achieve the mixture, renders an inhomogeneous solid.

The present work aims to produce a well-dispersed hybrid system composed of a carbon solid (Carbon Nanofiber or Graphene) and low loading levels of IF-WS_2. We found that to produce a well dispersed 3D structure of carbon nanofibers and IF-WS_2 it is necessary to employ the two stage *in situ* protocol described in the next section. In contrast, to produce a hybrid of Graphene (2D layered structure) with IF-WS_2, the use of the *in situ* protocol did not show significant improvement in the phase distribution when compared to physically mixing the components.

As an extension of the primary goals, we studied the mechanical properties of epoxy composites based on hybrid CNF/IF-WS_2 and G/IF-WS_2 made by *in situ* routes, and contrast the latter to those created from physical mixtures of the components.

2. Results and Discussion

With the goal of generating hybrid Carbon nanostructure/IF-WS_2 we conducted the steps summarized in the experimental section and produced samples whose qualities are described below. We have divided the results and discussion segment into three parts; the first one presenting the microstructural characteristics and stability of samples based on CNF/IF-WS_2, the second one including the study of Graphene/IF-WS_2 and the third showing the mechanical properties of both CNF/IF-WS_2 and Graphene/IF-WS_2 epoxy composites. The samples made in the absence of polymer were denominated hybrids and the ones with nanostructures embedded in epoxy are referred as composites as a way to distinguish them.

2.1. Carbon Nanofiber/IF-WS_2 Hybrids

The combination of existing 3D CNF structures with IF-WS_2 in the absence of a polymeric matrix, as mentioned in the introduction section, results in inhomogeneous solids. For example, the addition of IF-WS_2 to already existing CNF generates samples where diffusion paths dominate the final structure: the surface of the carbon fibers tends to contain larger amounts of the IF-WS_2 phase than sections of the sample not exposed to the surface. The use of solvents and sonication to disperse the IF or its precursors, is not enough to produce a homogeneous product. A second example; The addition of metal catalyst particles (to promote the carbon fiber growth) to existing IF-WS_2 followed by thermal treatments to proceed with the carbon nanofibers growth in the presence of a carbon source, produces a thin layer of metal sulfides in the surface of the metal particles. This phenomenon is observed also in the absence of carbon sources: at moderate temperatures (below 350 °C according to our findings) the metal reacts with the tungsten sulfide producing thin films of secondary phases in the metal particle surface, which in practice poison the catalyst, capping it and hindering the growth of the carbon fibers. Hence, this method also fails to produce the expected product. Variations in the experimental parameters, such as gas flows, placement of precursors, size and nature of metal catalyst, amid others, generates, in the best case scenario, amorphous carbonaceous byproducts of different sizes and morphologies, far from the desired fiber or porous structures [47].

Diverse precursor options could be used to generate IF-WS_2 structures; $(NH_4)_2WS_4$ thermal decomposition and WO_3 reaction with sulfur-containing compounds are among the most common routes employed [1,48–56]. The generation of IF-WS_2 carried out in our laboratories using such precursors resulted in samples with different levels of long range order and particle size, as can be

inferred from its XRD pattern and SEM analysis. Figure 1 presents the WS_2 patterns obtained when decomposing $(NH_4)_2WS_4$ and from the reaction of commercial WO_3 nanoparticles with H_2S atmospheres. It is worth noting that the temperatures needed for such reactions to occur differ, the former was performed at moderate temperatures (*ca.* 500 °C) while the latter required higher temperatures to be carried out to completion (*ca.* 800 °C). The diffraction peaks for IF-WS_2 generated from WO_3 are narrower and the reflections (00l) with l = 2*n* more evident and well defined than the ones obtained from $(NH_4)_2WS_4$. SEM observation of both products confirmed the presence of the hollow cage structures, the so-called 3R phase. Moreover, the former tetrathiotungstate precursor reacts with metal particles when it decomposes, which makes WO_3 the best choice to be combined with metal catalyst for fiber growth.

The two stage *in situ* synthesis of homogeneous CNF/IF-WS_2 required diverse atmospheres and temperature steps to be accomplished successfully. The first stage had the objective to grow CNF from a metal catalyst intermixed with WO_3 and the second stage consisted on sulfurizing the mixture of CNF/WO_3 to transform the tungsten oxide into IF-WS_2.

The dispersion of the metal particle (nickel in this case) with the WO_3 nanoparticles was performed using a solvent and sonication, followed by evaporating the mixture until dry since it rendered a more homogenous precursor than simply grinding the solids. A first temperature step was carried out at 350 °C in reducing atmospheres as a precautionary measure to assure that the metal catalyst surface was free of oxides. A second step at the same temperature including ethylene (as carbon source) and small amounts of oxygen diluted in inert gas (as reaction initiator and radical originator) was performed to cover the metal particle with an initial thin layer of carbon (which prevents the metal gross agglomeration and sintering at higher temperatures). The growth step was made at 550 °C, following protocols previously developed [57]. A final temperature stage at 900 °C in H_2S containing environment was included to transform the WO_3, now dispersed in between carbon nanofibers, into IF-WS_2. The sample was then allowed to cool to room temperature using an inert atmosphere.

Figure 1. XRD patterns of IF-WS_2 particles generated from different precursors. IF-WS_2 generated from (**a**) commercial WO_3 particles; (**b**) from ammonium tetrathiotungstate. All peaks were identified as IF-WS_2 [12].

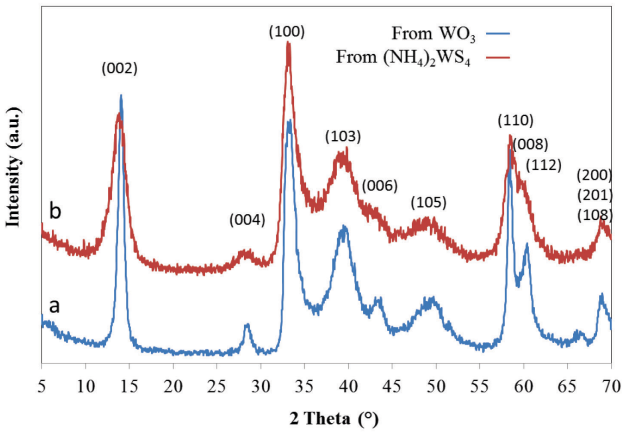

The electron micrographs of the nickel nanoparticles employed, the carbon nanotube intertwined nanofibers generated and the hybrid CNF/IF-WS_2 are presented in Figure 2. The ratios of catalyst to

WO_3 used were designed to have nominal loading values of 0.5, 1.5, and 5% of IF-WS_2 with respect to the total weight of the CNF. The distribution of the IF particles was studied using SEM in Secondary Electron (SE) and Backscattered Electron (BSE) modes along with Energy Dispersive Spectroscopy (EDS) mapping and can be described as discrete pockets of cage like particulates of approximately 1–2 microns dispersed into the CNF threads (Figure 2c). This finding is consistent across different sample locations.

The catalyst used for the carbon nanofibers was not removed and represents close to 3% of the total weight of the sample. Its effects on the properties of the epoxy composites are discussed in Section 2.3.

The last stage of the *in situ* protocol, the sulfurization, transforms not only the WO_3 into WS_2 but the nickel catalyst into nickel sulfide. Indeed, the hybrid CNF/IF-WS_2 samples are composed by the solids mentioned in Table 1 (experimental section), where nominal values and elemental analysis by ICP methods are contrasted. The inductive plasma emission spectroscopic data shows that the final composition attained is within 0.2% of the targeted values.

As a means to understand the characteristics of the samples and the different phases formed at the diverse synthesis steps, some of the runs where halted before completion and the products at that point, were analyzed by diverse techniques. As part of those trials, experiments of fiber growth in the absence of WO_3 with and without sulfurization treatment were performed. The X-ray diffraction analysis of the latter, containing only CNF samples, is presented in Figure 3. The main reflection, close to 26°, corresponds to the (002) peak of graphite, characteristic of many carbon products that include a crystalline component with various degrees of basal plane alignment [58]. In the present case the peak is associated to the CNF presence. The diffraction pattern of samples after the carbon fiber growth step but before sulfurization (red line in Figure 3), show only the peaks of graphite and a couple of reflections, close to 45 and 52°, that correspond to the nickel particles used as catalyst. The phases encountered after sulfurization (blue line) corroborate the presence of two extra crystalline structures, nickel sulfide: Ni_3S_2 [59,60] and $Ni_{17}S_{18}$ [61].

Figure 2. Microstructural Analysis of CNF and WS_2 precursors and CNF/IF-WS_2 hybrid**.** Scanning Electron Microscopy secondary electron images of (**a**) starting nickel nanoparticles; (**b**) carbon nanofibers grown from Ni catalyst; (**c**) nanoparticle dispersion and cluster of WS_2 nanoparticles within carbon nanofibers (CNF/IF-WS_2 hybrid).

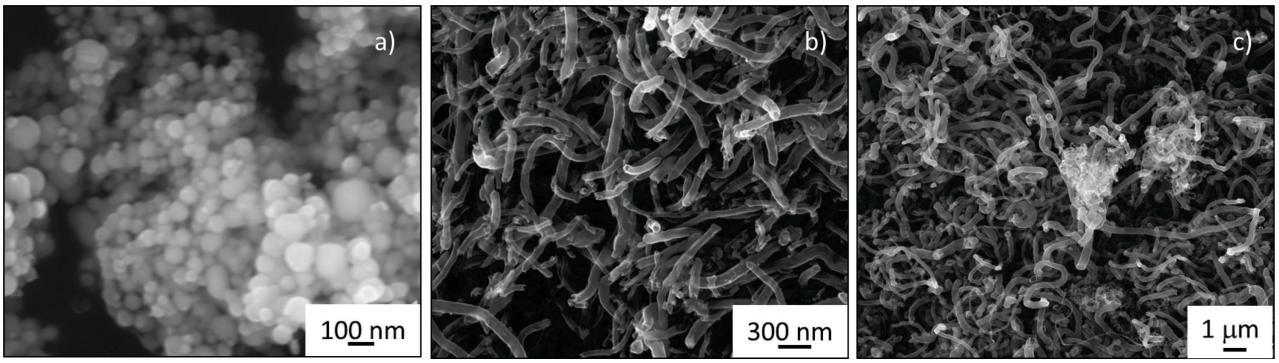

Figure 3. X-ray diffraction pattern of carbon nanofibers. (**a**) Typical peaks of graphite and nickel metal are identified in samples as prepared; (**b**) XRD pattern after sulfurization step shows graphite and nickel sulfide reflections.

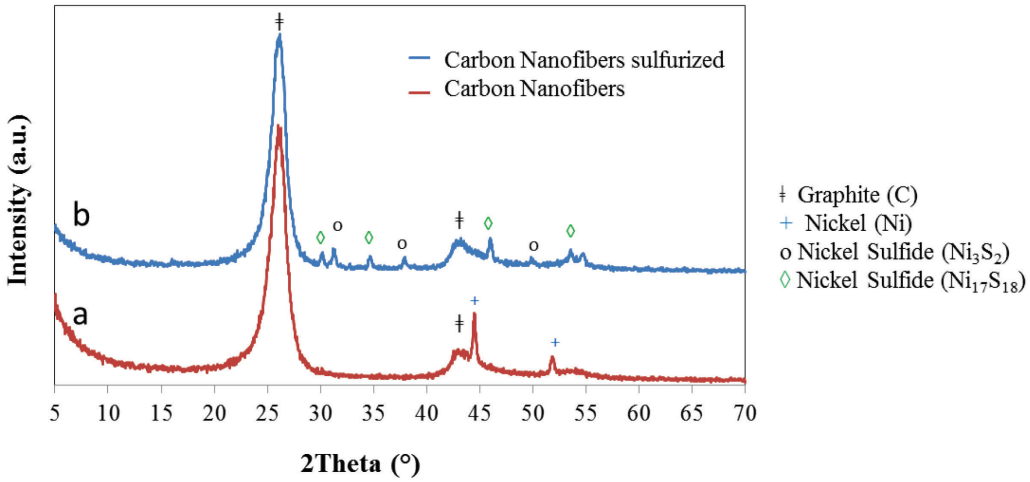

The XRD patterns of CNF/IF-WS_2 hybrids at the three different levels of loadings prepared are shown in Figure 4. The same phases recognized in Figure 3 after sulfurization; graphitic peaks, Ni_3S_2 and $Ni_{17}S_{18}$, along with a comparatively weak peak corresponding to IF-WS_2, can be identified.

Figure 4. X-ray diffraction patterns for hybrid CNF/IF-WS_2 samples. The main difference between XRD patterns in samples at diverse loadings is the relative intensity for the nickel sulfide *vs.* graphitic peaks.

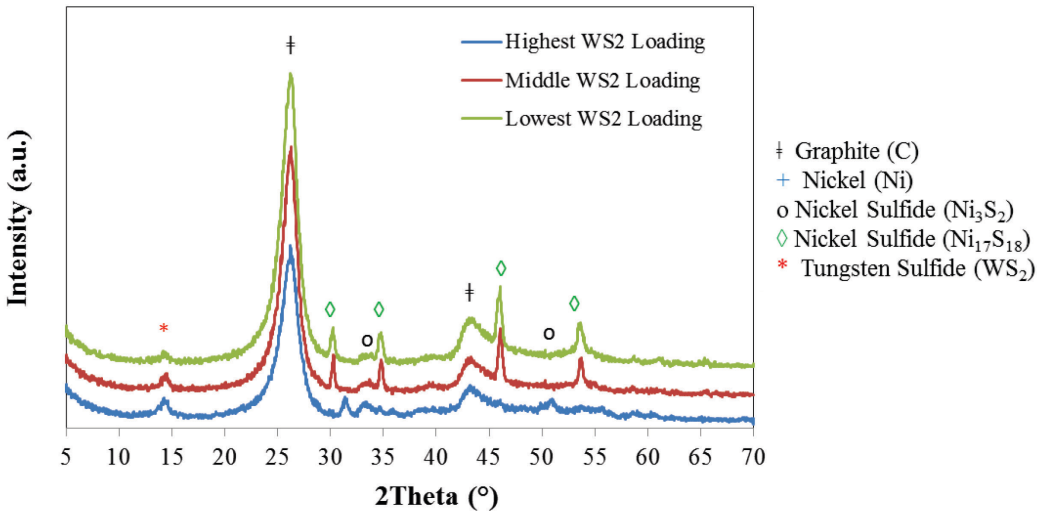

SEM in BSE mode studies along elemental mapping by EDX confirmed the presence of IF-WS_2 as highly dispersed phase. Figure 5 shows the metal distribution as bright spots (top left), including both nickel and tungsten phases. The IF-WS_2 distribution can be inferred as the positions where W elemental mapping is found (top right). The W mapping shows the presence of mainly small (nm) particulates homogeneously distributed in the sample. In contrast, the Ni particles used as catalyst,

now converted into sulfides, appear both as nanometer particulates and micron size agglomerates; with dimensions that could be correlated with the different fiber diameters (bottom right). The fact that the nickel elemental distribution shows micron size clusters is a sign that some agglomeration of some of the initial particles might have occurred during the fiber growth, since the original catalyst had a size distribution in the nm range, as shown in Figure 2a. The sulfur map (bottom left) encompasses both, the IF-WS_2 and Ni sulfide components.

Figure 5. Phase distribution studied by SEM/EDX analysis. **Top left**: Backscattered electron image showing the carbon fibers in grey and the metal containing phases as bright spots in the sample CNF/IF-WS_2 with the lowest IF-WS_2 loading. Elemental mapping by EDX analysis confirmed the presence of IF-WS_2 mainly as highly dispersed phase (**top right**) with small (nm) particle size. The elemental Ni map shows the presence of nm and micron size particulates (**bottom right**). The sulfur map (**bottom left**) includes both, the IF-WS_2 and Ni sulfide components.

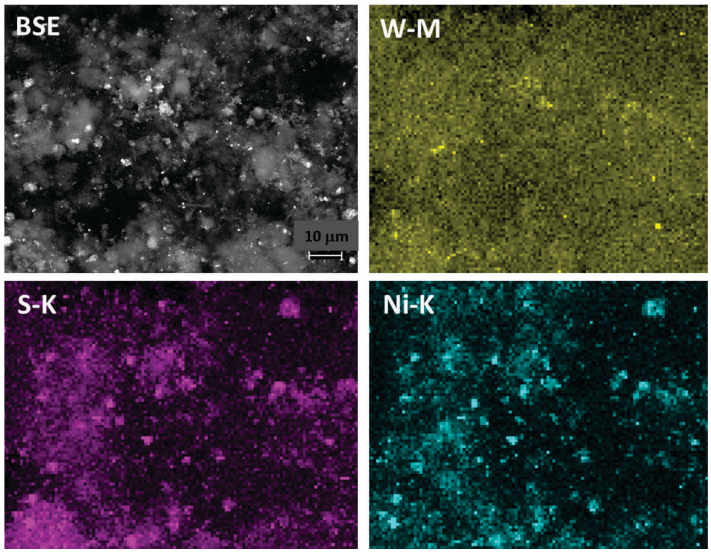

The samples' thermal analysis under oxygen containing atmospheres show that all specimens; CNF (catalyst included), CNF sulfurized and hybrid CNF/IF-WS_2 are stable at least up to a temperature of 500 °C (Figure 6). At higher temperatures the carbonaceous component burns off to produce CO_2, the tungsten sulfide reverts to its oxidized form and the metal catalyst oxidizes. Experiments conducted in inert atmosphere showed that hybrid CNF/IF-WS_2 samples do not present weight changes in the window of conditions used (RT to 950 °C) and can be considered thermally stable. Indeed, the hybrid samples stability observed surpasses the ones observed for polymer products without WS_2, which in either atmosphere start decomposing at much lower temperatures, and are in agreement with stability observed in air for IF-WS_2 based composites [19,20,62]. The reported thermal stability of WS_2 fullerene-like particles alone under oxidizing atmospheres indicates that, depending on particle size, oxidation might begin close to 290 °C (100 nm) or delay up to close to 440 °C (3 m), while exposed to inert gases the phase is stable up to 1200 °C [63,64]. In our case, the use of CNF without polymeric component seems to increase the thermal stability of the hybrid, given that the average IF-WS_2 particle size produced was in the nanometer scale (expected to oxidize close to

300 °C) and changes in weight were not evident until above ~500 °C. The thermal stability observed for IF-WS_2 might be related to the particulates being embedded in the CNF intertwined fibers, which might delay their reaction. Further studies to fully explain these phenomena are currently under way.

Figure 6. Thermogravimetric Analysis. Temperature programmed oxidation (burn off process) for (**a**) carbon nanofibers-including nickel catalyst; (**b**) sulfurized carbon nanofibers -including nickel sulfide and (**c**) CNF/IF-WS_2 hybrid with 3% tungsten sulfide loading. All of the samples are stable in oxygen containing environment up to 500 °C.

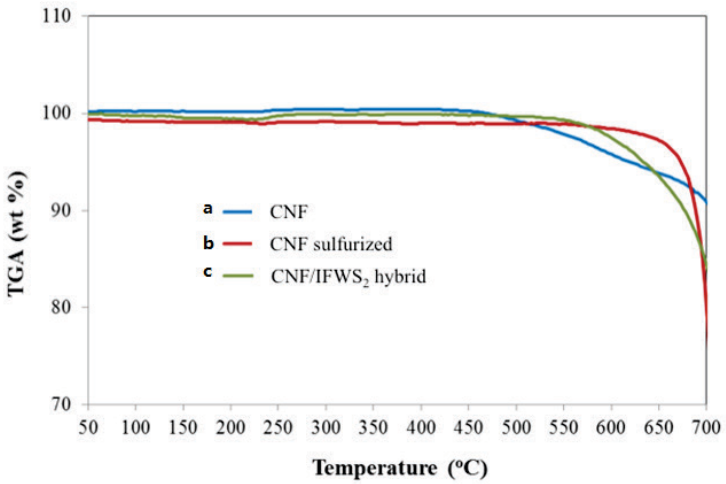

2.2. IF-WS_2/Graphene Hybrids

The complications introduced by the use of metal catalyst for nanofibers growth were not encountered during the synthesis of Graphene/IF-WS_2 hybrids, since no extra metal components were needed to generate them. Only small amounts of urea were used as an expansion agent. The production of graphene was accomplished by the reduction-expansion of graphite oxide (GO), which was generated from graphite flakes by the process described in the experimental section. The GO mediated process generates disordered graphene; where graphene sheets tend to entangle with each other but remain separated enough to maintain a relative high surface area (*ca.* 600 m^2/g as per BET analysis). It is worth noting that the oxygen content in the synthesis environment when using GO as a carbon precursor is sufficient to oxidize some of the IF-WS_2 if the latter is used since the beginning of the protocol, forcing the use of WO_3 as the tungsten source. Thus, WO_3 nanoparticles were subject to H_2S treatments to sulfurize them after its mixtures with graphene were obtained.

The two variations on the synthesis conditions consisted of: (i) dispersing the WO_3 nanoparticles with GO and then performing the exfoliation at high temperature (to generate Graphene/WO_3) followed by sulfurization (to obtain Graphene/IF-WS_2) or (ii) perform the GO exfoliation first and then directly mixing the resulting graphene with WO_3 and then sulfurizing the product (rendered Graphene/IF-WS_2). The microstructures created are presented in Figure 7.

The first synthetic approach, GO plus WO_3 exfoliation followed by sulfurization, resulted in hybrid Graphene/IF-WS_2 where the IF structures were located on the surface of disordered graphene sheets (marked by arrows, Figure 7a). Due to the thermal exfoliation and urea reduction process, when volatile groups leave the graphite oxide structure at temperatures close to 200 °C, they carry

along the WO_3, which ends in top of the layers, where they remain through the sulfurization step that converts them into IF-WS_2 cage structures. The exfoliation process separates the graphene sheets but also promotes the separation of IF particles, which were found in all cases as individual particles.

The position of the IF particulates following the second synthetic approach, is quite distinct. In this protocol, GO is first thermally exfoliated and reduced and the subsequent graphene is mixed with WO_3 (with the aid of solvents and sonication, followed by solvent evaporation until dry) and the mixture is then sulfurized. The IF particulates are found between the graphene layers, intimately embedded into the sheets structure (Figure 7b). Small (few nm diameter) IF particulate agglomerates, marked in the image with a blue arrow, were observed along individual particles, indicated by red arrows. The IF-WS_2 observed by Transmission Electron Microscopy presents the characteristic hollow cage, partially faceted structure and an interlayer spacing of 0.62 nm.

For comparison, samples in which Graphene and IF-WS_2 were formed as individual phases and then added as a physical mixture using solvents and sonication (not grown *in situ*), present similar structures to the ones in Figure 7b, demonstrating that the protocols developed to introduce IF-WS_2 into carbon structures are required only when tridimensional architectures of the carbonaceous component are needed but not if a layered, two dimensional structure is used.

Figure 7. Microstructural Analysis of Graphene/IF-WS_2 hybrids and IF-WS_2. Scanning Electron Microscopy images of (**a**) Graphene/IF-WS_2 hybrid generated from GO and WO_3; (**b**) Graphene/IF-WS_2 hybrid made directly from Graphene and WO_3; and (**c**) Transmission electron micrograph showing the characteristic hollow core and interlayer spacing for IF-WS_2 particles.

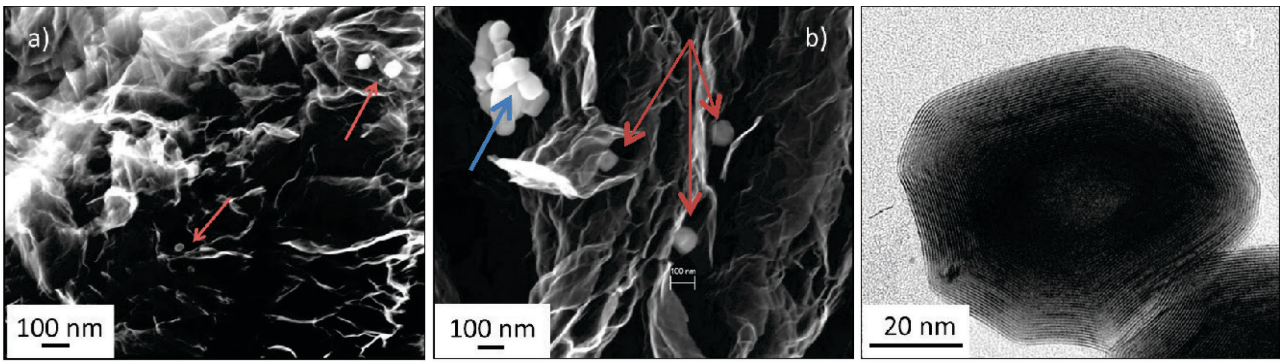

2.3. Epoxy Composites

The use of epoxy as polymeric matrix was intended (independent of its properties as a composite for use in protection systems) to determine the mechanical properties observed when using carbon nanomaterials with 3D *vs.* 2D structures (CNF *vs.* Graphene) that included low loadings of IF-WS_2. Other instances of WS_2 nanostructures embedded in epoxy can be found in [14,23], where WS_2 nanotubes were used as filler instead of the IF particulates used in this study. To the best of our knowledge, the only existing references including IF-WS_2 particles in epoxy systems do not involve a carbonaceous component [21–24].

Experimental testing in our laboratory and previous epoxy resin composite research data [47,65] were used to select 1% as targeted loading of filler material into epoxy matrix. Bare epoxy resin,

produced in identical conditions to the ones containing diverse fillers, was used as reference. Table 1 presents the values for the different filler components used to prepare the composites, all cases include only 1% of total filler and 99% of epoxy, by weight. On the table, the first column contains the nominal values of IF-WS_2 component targeted during synthesis, the rest of the columns are the values encountered when analyzing the filler samples by ICP Emission Spectroscopy.

Two types of nanoindentation measurements showed clear increases in the Young's modulus of the epoxy-CNF composites. As described in the experimental section, dynamic mechanical analysis was performed on epoxy-CNF composites to ascertain the degree of viscoelastic deformation of these materials at room temperature. At loading frequencies of both 1 Hz and 45 Hz, the elastic modulus response was dominated by the storage (elastic) modulus with a very minor contribution, less than 5%, from the loss (viscous) modulus. As such, quasi-static indentation was deemed appropriate for these materials. We used quasi-static nanoindention to measure the Young's modulus and hardness for each of the composites using the conditions listed in Table 2. The inclusion of carbon nanofibers into the epoxy matrix increases the epoxy modulus by 29%. CNF sulfurized, with no IF-WS_2 but subject to sulfurization process with H_2S, improves it nearly by 52% (Figure 8a). A possible explanation to the higher modulus values for the later might be related to the presence of sulfur and its effects on the epoxy-CNF interface adhesion. The three hybrid samples tested, CNF containing IF-WS_2 particulates with 0.5, 1.5, and 3%, show much higher modulus than the rest, with values that almost double the one for bare epoxy (for hybrid CNF/IF-WS_2 0.5%). While we observed a clear variation in sample performance for hybrids containing CNF and diverse IF-WS_2 contents, the data does not show a clear correlation with the actual amount of IF added.

For all samples that included fillers we observed a more dramatic change in hardness than for the elastic modulus; the initial addition of carbon nanofibers had a large effect and increased the hardness by more than 114% (Figure 8b). The addition of sulfurized fibers further raised the hardness by another 38%. The sulfurization of the fibers appears to improve the ability of the fibers to bond with the epoxy matrix, further improving the interfacial strength. The increase in hardness could also be partially due to the inclusion of nickel sulfide particles. As shown in Figures 3 and 4, after the sulfurization step is carried out all nickel used as catalyst for the CNF growth transforms into Ni_3S_2 or $Ni_{17}S_{18}$. While these particles contribute to an increase in performance in this case, it is possible that other effects could appear under different situations.

Nickel sulfide contamination is an ongoing concern for the tempered glass industry. High temperature structures of nickel sulfide can develop in the glass manufacturing process and become included in tempered glass. This inclusion will result in a stress concentration and if the particle is of a certain size, the pane of glass will shatter under loading far below what is expected of the material [66]. Depending on the future inclusions of these materials into other matrixes, the possible impact of sulfide particles as stress concentrators should be considered and further studied. In the case of polymeric matrices, like the ones studied herein, no failure modes related to the existence of nickel sulfide are expected, since the working and processing temperatures do not reach those where the nickel sulfide high temperature phase appears (715 °C). In the case of hybrids in the absence of polymers, the porous carbon fiber structure is presumed to accommodate the volume expansion of the phase change and does not constitute a concern.

All the hybrid CNF/IF-WS_2 samples showed a significant increment in hardness values, being CNF/IF-WS_2 0.5% the most remarkable, with a 247% improvement over the pure epoxy hardness.

Figure 8. Mechanical properties of epoxy composites. All composites contained 99% epoxy and 1% loading of filler nanostructures: CNF, sulfurized CNF or hybrid CNF/IF-WS_2. For the later, the hybrids contained mostly carbon fibers, with only 0.5, 1.5, and 3% of IF-WS_2. (**a**) Modulus data and (**b**) Hardness values.

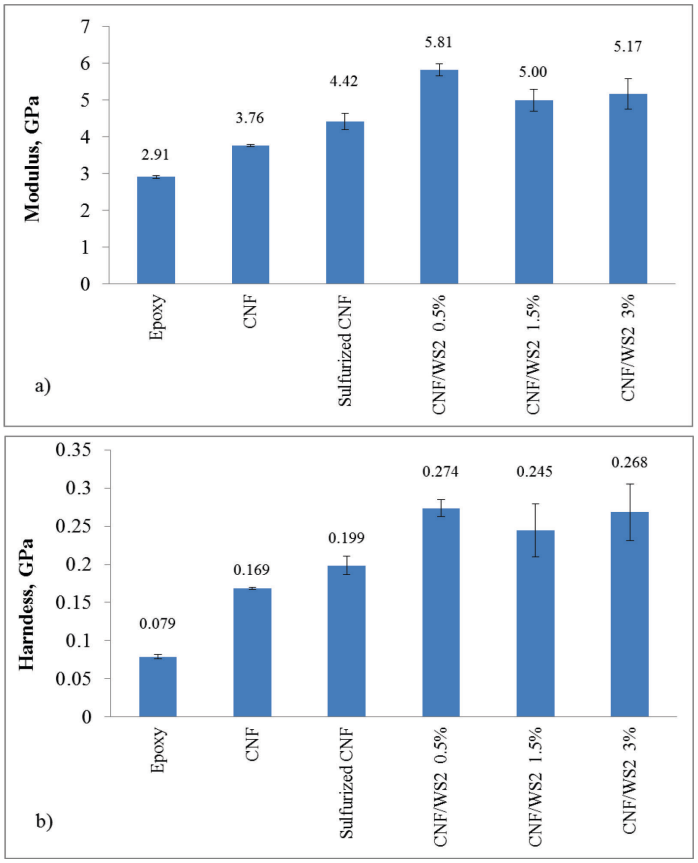

In order to fully understand the CNF/IF-WS_2 epoxy composite mechanical properties observed, further study of their interfaces by IR or other spectroscopic techniques is recommended. Such data will help characterize the changes introduced by the inorganic components in the oxirane ring bands, the overall epoxy resin structure and its degree of polymerization.

The inclusion of two-dimensional graphene into the epoxy matrix in equal loadings than the ones described above, 1wt% filler in epoxy, by itself or as Graphene/IF-WS_2, resulted in increased values of modulus and hardness (Figure 9). However, the improvement when compared to the 3D nanofiber structures is modest; the hybrid Graphene/IF-WS_2 with 0.5% of IF-WS_2 showed a 9% modulus increment over bare epoxy and a 47% increase in hardness. Histograms for the composites that contain CNF have been highlighted in blue and the ones containing graphene in red. From the Figure is clear that the samples based in 3D CNF architectures containing IF-WS_2 present the highest values. During the composite fabrication, the graphene based samples seemed to be more difficult to disperse into the epoxy matrices than the CNF ones and inconsistencies in the sample distribution into the epoxy puck might have a detrimental effect on the mechanical properties values. Moreover, the fact that the graphene sheets were distributed randomly in the sample and not oriented in the (002)

direction, where the strong covalent bonds are located, might be another point to be considered to explain the observed mechanical behavior.

As mentioned in Section 2.2, the use of Graphene/IF-WS_2 prepared *in situ vs*. the components physical mixtures do not seem to present an advantage in terms of phases distribution or their microstructural characteristics. In terms of mechanical properties, the *in situ* route and the physical mixtures of Graphene/IF-WS_2 are comparable; the values for modulus are almost the same and the hardness is higher for the former. This result might be related to the fact that IF particulates might easily disperse in between the graphene sheets without the need of a multistep process. It is worth noting that in the sample created *in situ*, the graphene structure has been exposed to H_2S atmospheres, while in the physical mixture the graphene was pristine and never in contact with sulfurizing environments. Given that the improvement in modulus and hardness over neat epoxy observed in those samples was minimal, the present study did not further investigate the interfacial effects created by diverse functionalities in the graphene surface.

Figure 9. Mechanical properties of epoxy composites. with 1% loading of CNF, sulfurized CNF, Graphene, IF-WS_2, CNT/IF-WS_2 hybrids or Graphene/IF-WS_2 hybrids. (**a**) Normalized Modulus data; (**b**) Normalized Hardness values.

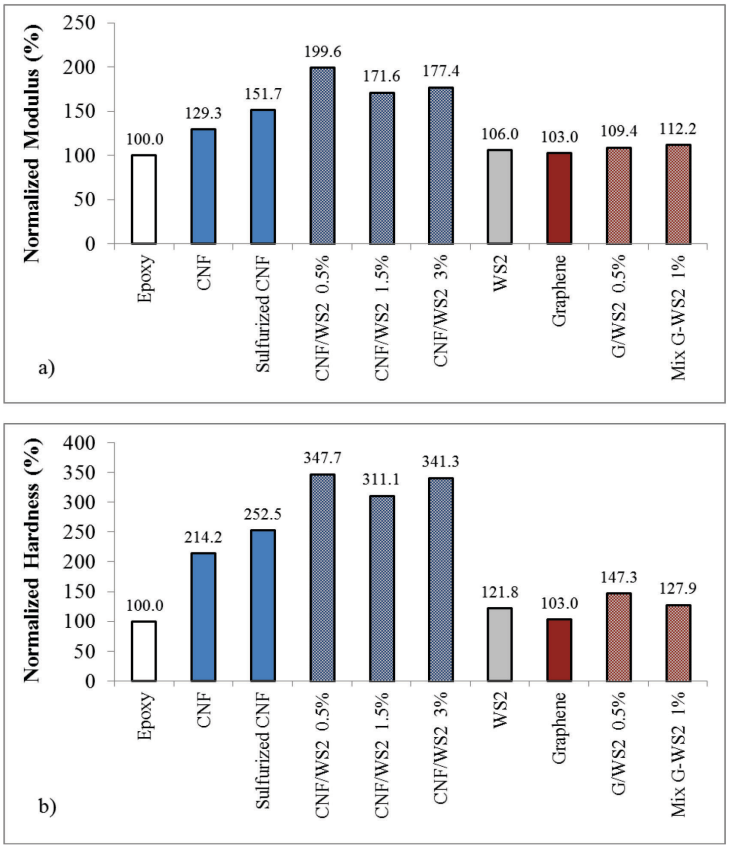

Overall, the epoxy composite samples containing 3D CNF structures along IF-WS_2 created *in situ*, showed drastic improvements in the Young's modulus and hardness values by the use of only 1% hybrid weight loadings. The carbon nanofiber inclusions seem to have a much greater impact in the mechanical properties of the composite than the graphene based counterparts for similar IF loadings.

The values for modulus and hardness improvements over the bare polymer mentioned above for CNF/IF-WS_2 composites surpass the ones encountered for other hybrid polymeric nanocomposites incorporating IF-WS_2 nanoparticles and a carbon phase [43–45]. However, in order to strictly compare mechanical properties for diverse fillers and polymeric matrices, data gathering should be performed under the same conditions and similar experimental setup to be valid. In particular, the use of nanoindentation instead of DMA tends to produce different values (usually larger for the former technique), as recently corroborated by Flores *et al*. [67]. Thus, comparison between the two techniques outcomes is not adequate given that no correlation between them exist to date.

3. Experimental Section

3.1. Carbon Nanofiber Hybrids/IF-WS_2

The amounts of IF-WS_2 included into CNF were determined by the knowledge gained in previous studies of composites by different groups [14,15,19], and consistent with the intent of generate lightweight materials, making the less dense carbon nanostructure component the most abundant phase. The multistep process employed to generate *in situ* structures is depicted in Figure 10.

Figure 10. CNF/IF-WS_2 preparation steps. Ni nanoparticles and WO_3 precursors were combined in solution using sonication in ethanol, dried and placed in a crucible inside a quartz tube of a tubular furnace. The mixture was then exposed to diverse environments and thermal treatments to generate Carbon Nanofiber/tungsten disulfide hybrids (CNF/IF-WS_2).

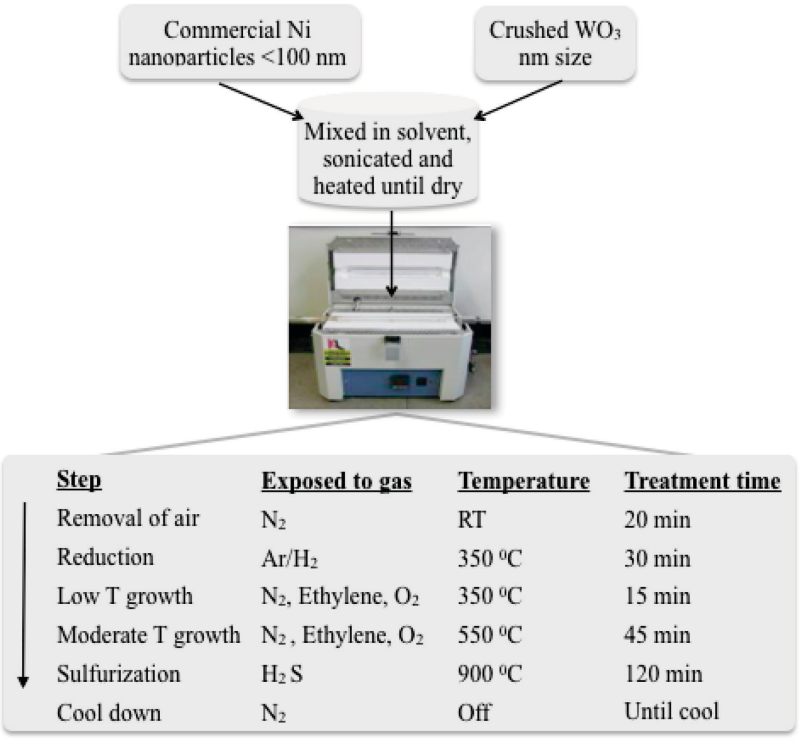

The gas flow rates employed for each step were: 300 sccm N_2 for air removal, 37 sccm of Ar/H_2 (93%/7%) for reduction, a mixture of 44 sccm N_2/15 sccm Ethylene/2 sccm O_2 for fiber growth (both low temperature and high), a mixture of 150 sccm N_2/15 sccm H_2S for sulfurization and 300 sccm N_2 during the cool down process.

3.2. IF-WS_2/Graphene Hybrids

The generation of graphene was performed in all cases starting from graphite flakes, which were oxidized to form graphite oxide (GO) following a modification of the process developed by Marcano *et al*. [68]. The GO was then used either as (i) dispersion with WO_3 nanoparticles and then exfoliated at high temperature with urea as expansion-reducing agent (to generate Graphene/WO_3) followed by a sulfurization step using H_2S atmosphere (to obtain Graphene/IF-WS_2) or (ii) exfoliated at high temperature with urea to form graphene, which was then mixed with WO_3 and the mixture sulfurized (this step rendered Graphene/IF-WS_2). The processes described are depicted in Figure 11.

Figure 11. Synthesis protocol followed to generate Graphene/IF-WS_2 hybrids from GO. Initial precursors (graphite flakes, acids and oxidant) will render graphite oxide. Protocols followed after GO generation (**i**) mixture of GO with WO_3 followed by exfoliation and sulfurization and (**ii**) Production of graphene through GO thermal exfoliation, mixture with WO_3 and sulfurization of mixture.

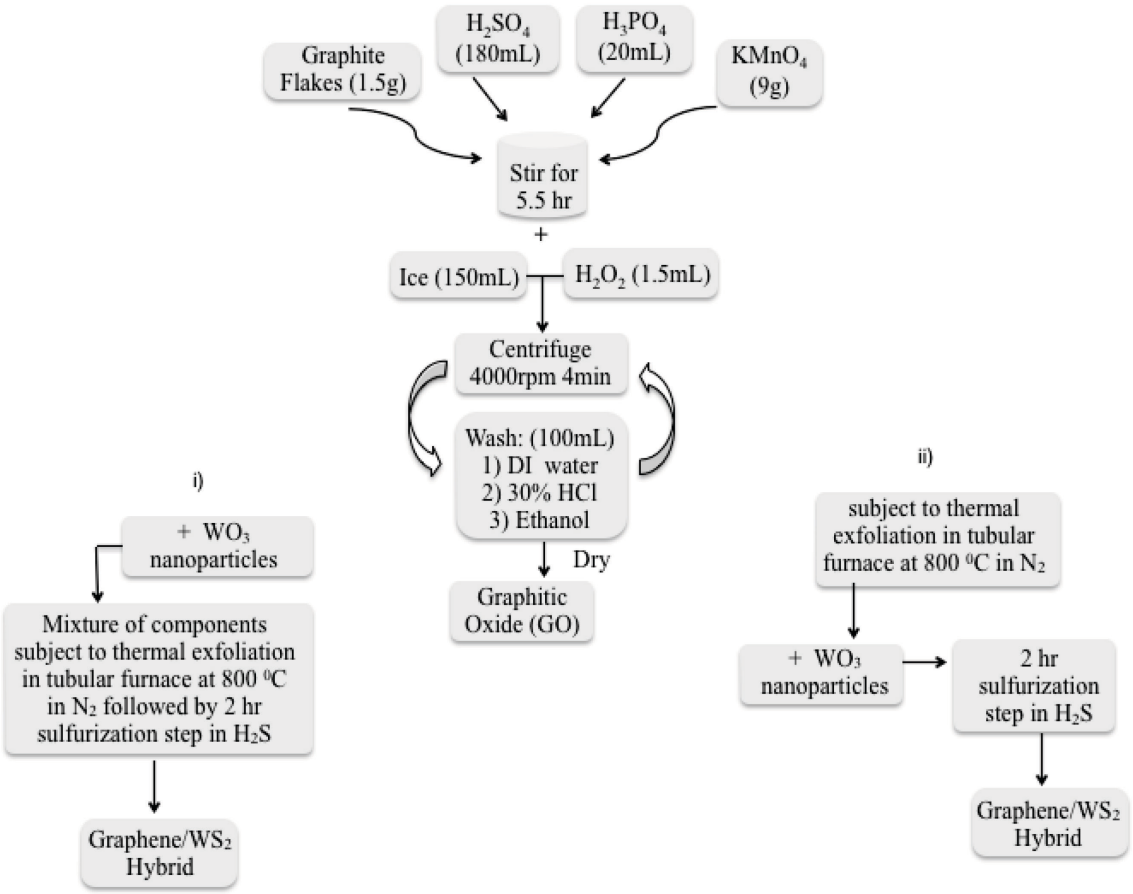

3.3. Epoxy Composites

We employed commercially available SpeciFix-20 (Struers, Ballerup, Denmark) as the epoxy resin, which consists of a resin and a hardening agent (26:5 ratio). Unlike some epoxies that require heating or pressure, this epoxy is designed to cure under atmospheric conditions. Further, it has a working period of 60 min, allowing time for the sample to be handled and nanocomposite added and mixed prior to the onset of curing. A loading of 1% nanoparticles to 99% epoxy by weight was selected for testing. The composition of the filler materials, the hybrids and individual phases described in previous sections, is included in Table 1 below. The filler components were added to the uncured resin using sonication and the composite was left for a period of at least 24 hours to cure into a hard puck. After the nanoparticles were successfully embedded into the epoxy matrix, the surface of the pucks was mechanically polished to remove scratches and imperfections and then transferred to the nanoindentor.

Table 1. Filler compositions used for epoxy composites (first column).

Sample ID (IF-WS_2 nominal composition – filler only)	**ICP value CNF**	**ICP value Ni**	**ICP value IF-WS_2**
CNF	96.8%	3.2%	
CNF/IF-WS_2 (3%)	94%	3%	3%
CNF/IF-WS_2 (1.5%)	94.6%	3.2%	1.6%
CNF/IF-WS_2 (0.5%)	96.4%	2.9%	0.7%
IF-WS_2 (100%)			100%
Sample ID (IFWS_2 nominal composition-filler only)	**Graphene**		**IF-WS_2**
Graphene	100%		
G/IF-WS_2 0.5%	99.5%		0.5%
Physical Mix G/IF-WS_2 1%	99%		1%

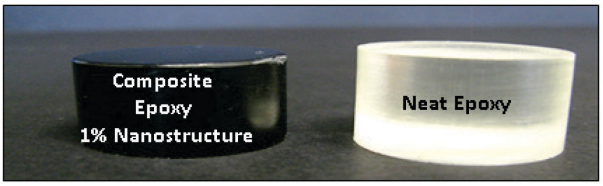

3.4. Characterization Methods

In order to examine the microstructure of the hybrid specimens the samples were analyzed using a Zeiss Neon 40 High Resolution Scanning Electron Microscope (SEM). Images were acquired at diverse magnifications while the microscope was operated at 10 or 20 kV. Energy Dispersive Spectroscopy (EDS) experiments were conducted in conjunction with the SEM using the EDAX equipment with an Apollo 10 silicon drift detector (SDD). Data was collected and analyzed using Genesis Spectrum software.

A Netzsch STA 449 FE Jupiter, operated in a Temperature Programmed Oxidation (TPO) mode, was used to study the thermal stability of the samples. The samples were exposed to an Ar/O_2, 80%/20% atmosphere, with a total flow of 120 mL minute^{-1}, from RT to 1000 °C at a heating rate of 10 °C minute^{-1}.

The XRD utilized was a Philips 1830 PAnalytical X-ray Diffractometer. The X-ray tube contained a copper source and the X-rays utilized had a primary wavelength, or K-Alpha, of 1.54 Å. The samples were placed into a silicon low background sample holder and the diffraction patterns recorded between 5–70° (2 theta) with 0.020 degrees step size and one second per step.

A JEOL 2010F FASTEM field emission gun scanning transmission electron microscope (STEM/TEM) equipped with Gatan GIF image filtering system was employed. Samples were prepared by dispersing the powders in a few ml of ethanol and a drop of the dispersion was placed in a copper holey-carbon TEM grid where the ethanol was allowed to evaporate.

A Perkin Elmer ICP 5300 DV-AES Inductive Coupled Plasma Emission Spectrometer, was used to determine the elemental composition of the carbon nanofiber base filler materials before their addition to the epoxy matrix (hybrids CNF/IF-WS_2).

Brunauer Emmet Teller (BET) surface area analysis was performed employing a Quantachrome Nova 4200. A 300 °C degas step was conducted prior to the analysis; samples were then allowed to cool down to room temperature and then transferred to the analysis station. The measurements were done using nitrogen atmosphere.

Nanoindentation was used to measure the composite mechanical properties (elastic modulus and hardness) of epoxy composites filled with mixtures of CNFs and IF-WS_2 particles. The samples were prepared by mixing the specified amounts of nanophase material with Struers Speci-Fix 20 two-part epoxy in a 28 mm diameter mold and then allowing the mixture to cure for 24 h. After curing, the surface of the epoxy composite was polished using standard metallographic techniques, including diamond suspension polishing using suspended aluminum oxide particles of 1 μm and 0.05 μm diameters. The indentations were performed using an Agilent G200 nanoindenter. We performed two types of experiments with this instrument.

The first experiment was a quasi-static indentation to a set depth, 2 μm for all samples. Other indentation parameters can be found in Table 2. This experiment used a diamond, Berkovich indenter tip with a nominal tip radius of 150 nm, calibrated using a fused silica standard. A grid of 20 indentation points spaced by 50 μm was measured for each epoxy nanocomposite. The Young's modulus and hardness were calculated using the approach of Oliver and Pharr [69,70].

Table 2. Parameters used for quasi-static indentation measurements.

Depth limit	2000 nm
Strain rate during loading	0.08/s
Maximum allowable drift rate	0.05 nm/s
Peak hold time	10 s
Assumed Poisson's ratio	0.40
% to unload	90
% Unload in stiffness calculation	50

The second experiment was dynamic mechanical analysis using a 50 μm diameter flat punch. This experiment allowed the measurement of both the storage and loss moduli of the epoxy composites. These measurements were performed for five frequency values between 1 Hz and 45 Hz on the neat epoxy, CNF and IF-WS_2 samples. Other parameters for the measurement can be found in Table 3. A grid of 20 measurements with a 100 μm separation between indentations was used for each specimen. The storage modulus, loss modulus, and tan δ properties for each specimen were calculated using the measurement parameters in Table 3 and the methods of Hay and Herbert [71].

Table 3. Parameters used for dynamic mechanical analysis.

Flat punch diameter	50 μm
Assumed Poisson's ratio	0.40
Pre-compression depth	2 μm
Oscillation amplitude	50 nm

4. Conclusions

Novel hybrid CNF/IF-WS_2 with diverse IF loadings were generated using an *in situ* protocol that allowed the integration of the two phases into a tridimensional architecture, producing homogeneous dispersions at the nanoscale in the absence of a polymeric matrix. CNF 3D structures loaded with IF-WS_2 could only be fabricated using a two stage process that involved: (a) the carbon nanofiber growth from a mixture of metal catalyst with tungsten oxide nanoparticles, using ethylene as carbon source and moderate temperatures to render CNF/WO_3, followed by (b) the sulfurization of the sample to convert the tungsten precursor into IF-WS_2.

In contrast, Graphene/IF-WS_2 hybrids were easily obtained either by mixing graphene and tungsten oxide followed by a sulfurization step or by direct dispersion of the layered graphene structure with existing IF particles using solvents.

The thermal stability of the CNF/IF-WS_2 hybrid samples is much higher than those observed for IF-WS_2 by itself or mixed with polymeric components.

Epoxy composites with 1% weight loadings of hybrid CNF/IF-WS_2 showed drastic improvements in the Young's modulus and hardness values, with approximately 100 and 250% increase respectively, over the bare epoxy values. The CNF/IF-WS_2 inclusions seem to have a much greater impact in the mechanical properties of the composite than the Graphene/IF-WS_2 based counterparts.

Acknowledgments

The work depicted in this manuscript has been possible with the support of the Office of Naval Research, Force Protection Thrust, Code 30. We appreciate the help of Dr. Abdul-Mehdi S. Ali from University of New Mexico, who conducted the analysis of the filler components elemental analysis by ICP. Our team is thankful for the HRTEM analysis of IF-WS_2 particles conducted by JEOL, USA Inc.

Conflicts of Interest

The authors declare no conflict of interest.

References

1. Margulis, L.; Tenne, R.; Iijima, S. Nucleation of WS_2 fullerenes at room temperature. *Microsc. Microanal. Microstruct.* **1996**, *7*, 87–89.
2. Rapoport, L.; Bilik, Y.; Feldman, Y.; Homyonfer, M.; Cohen, S.; Tenne, R. Hollow Nanoparticles of WS_2 as potential solid-state lubricants. *Nature* **1997**, *387*, 791–793.
3. Eidelman, O.; Friedman, H.; Tenne, R. Metallic films with fullerene-Like WS_2 (MoS_2) nanoparticles: Self-lubricating coatings with potential applications fullerene-like nanoparticles. In *Technological Innovations in Sensing and Detection of Chemical, Biological, Radiological, Nuclear Threats and Ecological Terrorism*; Springer: Dordrecht, Netherlands, 2012; pp. 59–67.
4. Rapoport, L.; Fleischer, N.; Tenne, R. Applications of WS_2 (MoS_2) inorganic nanotubes and fullerene-like nanoparticles for solid lubrication and for structural nanocomposites. *J. Mater. Chem.* **2005**, *15*, 1782–1788.
5. Drummond, C.; Alcantar, N.; Israelachvili, J.; Tenne, R.; Golan, Y. Microtribology and friction-induced material transfer in WS_2 nanoparticle additives. *Adv. Funct. Mater.* **2001**, *11*, 348–354.
6. Rothschild, A.; Cohen, S.; Tenne, R. WS_2 nanotubes as tips in scanning probe microscopy. *Appl. Phys. Lett.* **1999**, *75*, 4025–4027.
7. Dominko, R.; Arčon, D.; Mrzel, A.; Zorko, A.; Cevc, P.; Venturini, P.; Gaberscek, M.; Remskar, M.; Mihailovic, D. Dichalcogenide nanotube electrodes for li-ion batteries. *Adv. Mater.* **2002**, *14*, 1531–1534.
8. Cheng, F.Y.; Chen, J.; Gou, X.L. MoS_2/Ni Nanocomposites as catalysts for hydrodesulfurization of thiophene and thiophene derivatives. *Adv. Mater*. **2006**, *18*, 2561–2564.
9. Wang, Y.; Shi, Z.; Huang, Y.; Ma, Y.; Wang, C.; Chen, M.; Chen, Y. Supercapacitor devices based on graphene materials. *J. Phys. Chem.* **2009**, *113*, 13103–13107.
10. Zhu, Y.; Sekine, T.; Brigatti, K.; Firth, S.; Tenne, R.; Rosentsveig, R.; Kroto, H.; Walton, D. Shock-wave resistance of WS_2 nanotubes. *J. Am. Chem. Soc.* **2003**, *125*, 1329–1333.
11. Zhu, Y.; Sekine, T.; Li, Y.; Wang, W.; Fay, M.; Edwards, H.; Brown, P.; Fleischer, N.; Tenne, R. WS_2 and MoS_2 Inorganic fullerenes—super shock absorbers at very high pressures. *Adv. Mater*. **2005**, *17*, 1500–1503.
12. Zhu, Y.; Sekine, T.; Li, Y.; Fay, M.; Zhao, Y.; Poa, C.; Wang, W.; Roe, M.; Brown, P.; Fleischer, N.; *et al.* Shock-absorbing and failure mechanisms of WS_2 and MoS_2 nanoparticles with fullerene-like structures under shock wave pressure. *J. Am. Chem. Soc.* **2005**, *127*, 16263–16272.
13. Volkova, E.I.; Jones, I.A.; Brooks, R.; Zhu, Y.; Bichoutskaia, E. Meso-scale Modelling of Shock Wave Propagation in a SiC/Al nanocomposite reinforced with WS_2-inorganic fullerene nanoparticles. *Compos. Struct.* **2013**, *96*, 601–605.
14. Tehrani, M.; Luhrs, C.C.; Al-Haik, M.S.; Trevino, J.; Zea, H. Synthesis of WS_2 nanostructures from the reaction of WO_3 with CS_2 and mechanical characterization of WS_2 nanotube composites. *Nanotechnology* **2011**, *22*, 285714.

15. Naffakh, M.; Diez-Pascual, A.M.; Marco, C.; Ellis, G.J.; Gomez-Fatou, M.A. Opportunities and challenges in the use of inorganic fullerene-like Nanoparticles to Produce Advanced Polymer Nanocomposites. *Prog. Polym. Sci.* **2013**, *38*, 1163–1231.
16. Naffakh, M.; Diez-Pascual, A.M.; Gomez-Fatou, M.A. New Hybrid nanocomposites containing carbon nanotubes, inorganic fullerene-like WS_2 nanoparticles and poly(ether ether ketone) (PEEK). *J. Mater. Chem.* **2011**, *21*, 7425–7433.
17. Naffakh, M.; Diez-Pascual, A.M.; Marco, C.; Gomez, M.A.; Jimenez, I. Novel melt-processable poly (ether ether ketone) (PEEK)/inorganic fullerene-like WS_2 nanoparticles for critical applications. *J. Phys. Chem. B* **2010**, *114*, 11444–11453.
18. Diez-Pascual, A.M.; Naffakh, M.; Marco, C.; Ellis, G. Rheological and tribological properties of carbon nanotube/thermoplastic nanocomposites incorporating inorganic fullerene-Like WS_2 Nanoparticles. *J. Phys. Chem.* **2012**, *116*, 7959–7969.
19. Diez-Pascual, A.M.; Naffakh, M. Mechanical and thermal behaviour of isotactic polypropylene reinforced with inorganic fullerene-like WS_2 nanoparticles: Effect of Filler Loading and Temperature. *Mater. Chem. Phys.* **2013**, *141*, 979–989.
20. Ma, T.; Zhang, T.; Gao, P.G.; Zhang, J.C. Synthesis and properties of ultrahigh molecular weight polyethylene/WS_2 nanoparticle fiber for bullet-proof materials. *Chin. Sci. Bull*. **2013**, *58*, 945–948.
21. Shneider, M.; Dodiuk, H.; Tenne, R.; Kenig, S. Nanoinduced morphology and enhanced properties of epoxy containing tungsten disulfide nanoparticles. *Polym. Eng. Sci.* **2013**, *53*, 2624–2632.
22. Shneider, M.; Rapoport, L.; Moshkovich, A.; Dodiuk, H.; Kenig, S.; Tenne, R.; Zak, A. Tribological performance of the epoxy-based composite reinforced by WS_2 fullerene-like nanoparticles and nanotubes. *Phys. Status Solidi A* **2013**, *210*, 2298–2306.
23. Zohar, E.; Baruch, S.; Shneider, M.; Dodiuk, H.; Kenig, S.; Tenne, R.; Wagner, H.D. The Effect of WS_2 nanotubes on the properties of epoxy-based nanocomposites. *J. Adhes. Sci. Technol*. **2011**, *25*, 1603–1617.
24. Shneider, M.; Dodiuk, H.; Kenig, S.; Tenne, R. The Effect of Tungsten Sulfide Fullerene-Like Nanoparticles on the toughness of epoxy adhesives. *J. Adhes. Sci. Technol.* **2010**, *24*, 1083–1095.
25. Lalwani, G.; Kwaczala, A.T.; Kanakia, S.; Patel, S.C.; Judex, S.; Sitharaman, B. Fabrication and characterization of three-dimensional macroscopic all-carbon scaffolds. *Carbon* **2013**, *53*, 90–100.
26. Franklin, N.; Dai, H. An enhanced CVD approach to extensive nanotube networks with directionality. *Adv. Mater.* **2000**, *12*, 890–894.
27. Calvo, M.; Garcia, R.; Arenillas, A.; Suarez, I.; Moinelo, S. Carbon foams from coals. A preliminary study. *Fuel* **2005**, *84*, 2184–2189.
28. Calvo, M.; Garcia, R.; Moinelo, S.R. Carbon foams from different coals. *Energy Fuels* **2008**, *22*, 3376–3383.
29. Chen, C.; Kennel, E.; Stiller, A.; Stansberry, P.; Zondlo, J. Carbon foam derived from various precursors. *Carbon* **2006**, *44*, 1535–1543.

30. Chakrapani, N.; Wei, B.; Carrillo, A.; Ajayan, P.; Kane, R. Capillarity-driven assembly of two-dimensional cellular carbon nanotube foams. *Proc. Natl. Acad. Sci. USA* **2004**, *101*, 4009–4012.
31. Chakrapani, N.; Wei, B.; Carrillo, A.; Ajayan, P.; Kane, R. Capillarity-driven assembly of cellular carbon nanotube foams. *Abstr. Pap. Am. Chem. Soc.* **2004**, *228*, U481–U481.
32. Gallego, N.; Klett, J. Carbon Foams for Thermal Management. *Carbon* **2003**, *41*, 1461–1466.
33. Kaur, S.; Ajayan, P.M.; Kane, R.S. Design and characterization of three-dimensional carbon nanotube foams. *J. Phys. Chem. B* **2006**, *110*, 21377–21380.
34. Dai, L.; Patil, A.; Gong, X.; Guo, Z.; Liu, L.; Liu, Y.; Zhu, D. Aligned nanotubes. *Chemphyschem* **2003**, *4*, 1150–1169.
35. Atwater, M.A.; Mousavi, A.K.; Leseman, Z.C.; Phillips, J. Direct synthesis and characterization of a nonwoven structure comprised of carbon nanofibers. *Carbon* **2013**, *57*, 363–370.
36. Safdari, M.; Al-Haik, M.S. Optimization of stress wave propagation in a multilayered elastic/viscoelastic hybrid composite based on carbon fibers/carbon nanotubes. *Polym. Compos.* **2012**, *33*, 196–206.
37. Khalid, W.; Ali, M.S.M.; Dahmardeh, M.; Choi, Y.; Yaghoobi, P.; Nojeh, A.; Takahata, K. High-aspect-ratio, free-form patterning of carbon nanotube forests using micro-electro-discharge machining. *Diamond Relat. Mater*. **2010**, *19*, 1405–1410.
38. Qiu, L.; Liu, J.Z.; Chang, S.L.Y.; Wu, Y.; Li, D. Biomimetic superelastic graphene-based cellular monoliths. *Nat. Commun.* **2012**, *3*, 1241.
39. Geim, A.K.; Novoselov, K.S. The rise of graphene. *Nat. Mater.* **2007**, *6*, 183–191.
40. Stankovich, S.; Dikin, D.A.; Dommett, G.H.B.; Kohlhaas, K.M.; Zimney, E.J.; Stach, E.A.; Piner, R.D.; Nguyen, S.T.; Ruoff, R.S. Graphene-based composite materials. *Nature* **2006**, *442*, 282–286.
41. Naffakh, M.; Diez-Pascual, A.M.; Marco, C.; Ellis, G. Morphology and thermal properties of novel poly (phenylene sulfide) hybrid nanocomposites based on single-walled carbon nanotubes and inorganic fullerene-like WS_2 nanoparticles. *J. Mater. Chem*. **2012**, *22*, 1418–1425.
42. Diez-Pascual, A.M.; Naffakh, M.; Gomez-Fatou, M.A. Mechanical and electrical properties of novel poly(ether ether ketone)/carbon nanotube/inorganic fullerene-like WS_2 hybrid nanocomposites: Experimental measurements and theoretical predictions. *Mater. Chem. Phys.* **2011**, *130*, 126–133.
43. Diez-Pascual, A.M.; Naffakh, M. Inorganic Nanoparticle-Modified Poly(Phenylene Sulphide)/Carbon Fiber Laminates: Thermomechanical Behaviour. *Materials* **2013**, *6*, 3171–3193.
44. Diez-Pascual, A.M.; Naffakh, M. Tuning the properties of carbon fiber-reinforced poly (phenylene sulphide) laminates via incorporation of inorganic nanoparticles. *Polymer* **2012**, *53*, 2369–2378.
45. Diez-Pascual, A.M.; Naffakh, M.; Marco, C.; Ellis, G. Mechanical and electrical properties of carbon nanotube/poly(phenylene sulphide) composites incorporating polyetherimide and inorganic fullerene-like nanoparticles. *Compos. Part A* **2012**, *43*, 603–612.
46. Luhrs, C.C.; Daskam, C.D.; Gonzalez, E.; Phillips, J. Fabrication of a Low Density Carbon Fiber Foam and Its Characterization as a Strain Gauge. *Materials*, submitted for publication, 2014.
47. Moberg, M. Carbon Fiber and Tungsten Disulfide Nanoscale Architectures for Armor Applications. MS Thesis, Naval Postgraduate School, June 2012.

48. Feldman, Y.; Frey, G.; Homyonfer, M.; Lyakhovitskaya, V.; Margulis, L.; Cohen, H.; Hodes, G.; Hutchison, J.; Tenne, R. Bulk synthesis of inorganic fullerene-like MS_2 (M = Mo, W) from the respective trioxides and the reaction mechanism. *J. Am. Chem. Soc.* **1996**, *118*, 5362–5367.
49. Tenne, R.; Homyonfer, M.; Feldman, Y. Nanoparticles of layered compounds with hollow cage structures (inorganic fullerene-like structures). *Chem. Mater*. **1998**, 3225–3238.
50. Tenne, R.; Remskar, M.; Enyashin, A.; Seifert, G. Inorganic nanotubes and fullerene-like structures (IF). *Carbon Nanotubes* **2008**, *111*, 631–671.
51. Bar-Sadan, M.; Kaplan-Ashiri, I.; Tenne, R. Inorganic fullerenes and nanotubes: Wealth of materials and morphologies. *Eur. Phys. J.-Spec. Top.* **2007**, *149*, 71–101.
52. Wiesel, I.; Arbel, H.; Albu-Yaron, A.; Popovitz-Biro, R.; Gordon, J.M.; Feuermann, D.; Tenne, R. Synthesis of WS_2 and MoS_2 Fullerene-Like Nanoparticles from Solid Precursors. *Nano Res.* **2009**, *2*, 416–424.
53. Bastide, S.; Borra, J.; Duphil, D.; Levy-Clement, C. Synthesis of inorganic fullerenes and nanoboxes of MoS_2 and WS_2 by spray pyrolysis. *Abstr. Pap. Am. Chem. Soc*. **2004**, *228*, U482–U482.
54. Zink, N.; Pansiot, J.; Kieffer, J.; Therese, H.A.; Panthofer, M.; Rocker, F.; Kolb, U.; Tremel, W. Selective synthesis of hollow and filled fullerene-like (IF) WS_2 nanoparticles via metal-organic chemical vapor deposition. *Chem. Mater.* **2007**, 6391–6400.
55. Brooks, D.; Douthwaite, R.; Brydson, R.; Calvert, C.; Measures, M.; Watson, A. Synthesis of inorganic fullerene (MS_2, M = Zr, Hf and W) phases using H_2S and N_2/H_2 microwave-induced plasmas. *Nanotechnology* **2006**, *17*, 1245–1250.
56. Tenne, R. Inorganic nanotubes and fullerene-like nanoparticles. *Nat. Nanotechnol.* **2006**, *1*, 103–111.
57. Luhrs, C.C.; Garcia, D.; Tehrani, M.; Al-Haik, M.; Taha, M.R.; Phillips, J. Generation of carbon nanofilaments on carbon fibers at 550 degrees C. *Carbon* **2009**, *47*, 3071–3078.
58. Pierson, H.O. *Handbook of Carbon, Graphite, Diamond, and Fullerenes*; Noyes Publications: Park Ridge, NJ, USA, 1993.
59. Fleet, M.E. Crystal-Structure of Heazlewoodite, and Metallic Bonds in Sulfide Minerals. *Am. Mineral.* **1977**, *62*, 341–345.
60. Parise, J.B. Structure of Hazelwoodite (Ni_3S_2). *Acta Crystallogr. Sect. B* **1980**, *36*, 1179–1180.
61. Villars, P.; Cenzual, K. *Landolt-Bornstein—Group III Condensed Matter*; Springer: Berlin, Germany, 2010.
62. Xu, F.; Almeida, T.P.; Chang, H.; Xia, Y.; Wears, M.L.; Zhu, Y. Multi-walled carbon/IF-WS_2 nanoparticles with improved thermal properties. *Nanoscale* **2013**, *5*, 10504–10510.
63. Schuffenhauer, C.; Wildermuth, G.; Felsche, J.; Tenne, R. How stable are inorganic fullerene-like particles. Thermal analysis (STA) of inorganic fullerene-like NbS_2, MoS_2, and WS_2 in oxidizing and inert atmospheres in comparison with the bulk material. *Phys. Chem. Chem. Phys.* **2004**, *6*, 3991–4002.
64. Chang, L.; Yang, H.; Fu, W.; Yang, N.; Chen, J.; Li, M.; Zou, G.; Li, J. Synthesis and thermal stability of W/WS_2 inorganic fullerene-like nanoparticles with core-shell structure. *Mater. Res. Bull.* **2006**, *41*, 1242–1248.

65. Dutta, A.; Penumadu, D.; Files, B. Nanoindentation testing for evaluating modulus and hardness of single-walled carbon nanotube-reinforced epoxy composites. *J. Mater. Res.* **2004**, *19*, 158–164.
66. Gromowski, K. *Glass Breakage—Nickel Sulfide Inclusions*; Penn State: State College, PA, USA, 2010.
67. Flores, A.; Naffakh, M.; Diez-Pascual, A.M.; Ania, F.; Gomez-Fatou, M.A. Evaluating the Reinforcement of Inorganic Fullerene-like Nanoparticles in Thermoplastic Matrices by Depth-Sensing Indentation. *J. Phys. Chem. C* **2013**, *117*, 20936–20943.
68. Marcano, D.C.; Kosynkin, D.V.; Berlin, J.M.; Sinitskii, A.; Sun, Z.; Slesarev, A.; Alemany, L.B.; Lu, W.; Tour, J.M. Improved Synthesis of Graphene Oxide. *ACS Nano* **2010**, *4*, 4806–4814.
69. Oliver, W.; Pharr, G. An Improved Technique for Determining Hardness and Elastic-Modulus using Load and Displacement Sensing Indentation Experiments. *J. Mater. Res.* **1992**, *7*, 1564–1583.
70. Pharr, G.; Oliver, W.; Brotzen, F. On the Generality of the Relationship among Contact Stiffness, Contact Area, and Elastic-Modulus during Indentation. *J. Mater. Res.* **1992**, *7*, 613–617.
71. Hay, J.; Herbert, E. Measuring the Complex Modulus of Polymers by Instrumented Indentation Testing. *Exp. Tech.* **2013**, *37*, 55–61.